# Climate projections for selected large marine ecosystems

Muyin Wang [a,*], James E. Overland [b], Nicholas A. Bond [a]

[a] Joint Institute for the Study of the Atmosphere and Ocean, Box 355672, University of Washington, Seattle, WA 98195, USA
[b] Pacific Marine Environmental Laboratory, National Oceanic and Atmospheric Administration, 7600 Sand Point Way NE, Seattle WA 98115, USA

## ARTICLE INFO

## ABSTRACT

In preparation for the Intergovernmental Panel on Climate Change (IPCC) Fourth Assessment Report (AR4) modeling centers from around the world carried out sets of global climate simulations under various emission scenarios with a total of 23 coupled atmosphere–ocean general circulation models. We evaluated the models' 20th century hindcasts of selected variables relevant to several large marine ecosystems and examined 21st century projections by a subset of these models under the A1B (middle range) emission scenario. In general we find that a subset (about half) of the models are able to simulate large-scale aspects of the historical observations reasonably well, which provides some confidence in their application for projections of ocean conditions into the future. Over the North Pacific by the mid-21st century, the warming due to the trend in wintertime sea surface temperature (SST) will be 1°–1.5 °C, which is as large as the amplitude of the major mode of variability, the Pacific Decadal Oscillation (PDO). For areas northwest of the Hawaiian Islands, these models projected a steady increase of 1.2 °C in summer SST over the period from 2000 to 2050. For the Bering and Barents seas, a subset of models selected on the basis of their ability to simulate sea–ice area in late 20th century yield an average decrease in sea–ice coverage of 43% and 36%, respectively, by the decade centered on 2050 with a reasonable degree of consistency. On the other hand, model simulations of coastal upwelling for the California, Canary and Humboldt Currents, and of bottom temperatures in the Barents Sea, feature a relatively large degree of uncertainty. These results illustrate that 21st century projections for marine ecosystems in certain regions using present-generation climate models require additional analysis.

© 2009 Elsevier B.V. All rights reserved.

## 1. Introduction

Previous studies have shown that climate variations can cause significant changes in marine ecosystems (e.g. Livingston and Tjelmeland, 2000). The changes expected in the physical environment due to anthropogenic influences will have effects on ecosystems as well (Pierce, 2004). Over the North Pacific, for example, production cycles of the Alaskan salmon (*Oncorhynchus* spp.) are closely connected with the variations of the sea surface temperature (SST) (Beamish, 1993; Hare et al., 1999). The distribution and abundance in halibut (*Hippoglossus stenolepis*) in the Gulf of Alaska, sardine (*Sardinops melanostictus*) near Japan, and various species along the Oregon/California coast have also been shown to be related to climate shifts in the North Pacific (e.g. Clark and Hare, 2002). The health of the coral reef near Hawaii is sensitive to the maximum SST in late summer (August to October) (Hoeke et al., 2006). Over the Bering and Barents seas, climate variations are accompanied by substantial fluctuations in sea ice, with impacts on oceanographic and ecosystem properties throughout the year. Sea ice also provides essential habitat for marine mammals such as seals and walrus, and influences the timing of the spring bloom, with subsequent effects on higher trophic levels. Another example is Atlantic cod (*Gadus morhua*) which are found throughout the North Atlantic in waters with annual temperatures ranging from 0–12 °C (Drinkwater, 2005). As discussed by Sundby (2000), temperature influences Atlantic cod recruitment, their individual growth and their distribution.

In preparation for the Intergovernmental Panel on Climate Change Fourth Assessment Report (IPCC AR4), 17 international modeling centers submitted their hindcasts of 20th century climate from 23 models and the corresponding projections for the future under a suite of emission scenarios. The hindcasts incorporated external influences due to observed solar and volcanic variations as well as green house gas concentrations. These hindcasts, together with projections for the 21st century and beyond under different emissions scenarios are part of the phase 3 project, named "phase 3 of the Coupled Model Intercomparison Project (CMIP3)". In comparison to the Third Assessment report (TAR) published 6 years ago, a major change in the experimental design was to make the model outputs available to a large science community for independent evaluation. As part of this process we evaluated Arctic temperature hindcasts from 20 models for the 20th century (Wang et al., 2007a) and found that about half of the models provided some confidence in resolving decadal variability. For the

North Pacific, 10 out of 18 models reproduced the salient spatial and temporal aspects of the primary mode of variability, the Pacific Decadal Oscillation (PDO) (Overland and Wang, 2007a). With regards to sea–ice simulations: 11 of out 20 models yield ice areas for the northern hemisphere summer similar to the observed values (Overland and Wang, 2007b). On a regional basis, however, a smaller fraction of the models are able to replicate the observed sea–ice areas, and different models demonstrate skill in different regions. This result motivated us to further investigate the feasibility of applying the climate simulations from these CMIP3 models to selected Large Marine Ecosystems (LME).

The principal objective of the present study is to analyze CMIP3 model results of physical properties relevant to LMEs. We employ examples of the North Pacific as a whole at the beginning. The regions northwest of Hawaii Islands, the Bering Sea, three eastern boundary currents regions featuring coastal upwelling (the California, Canary and Humboldt Currents), and the Barents and the North Sea in North Atlantic are considered. Our analysis can be considered as a first step towards projecting likely changes in these ecosystems over the next 30–50 years. A crucial aspect of these projections is their reliability. As will be shown below, based on the CMIP3 model outputs themselves, the reliability varies between regions. The processes that control ecosystem structure and function differ among the regions, and these processes are not equally predictable. The examples considered here illustrate the complexity in model evaluation process and the importance of doing so.

The paper is organized as follows. The next section consists of a brief description of the models used in analysis. We then present results for the various LMEs. We conclude with a summary and a discussion of issues associated with the application of CMIP3 model simulations for LMEs.

## 2. Model sources

The model output used in our analysis is from the archive maintained by the Program for Climate Model Diagnosis and Intercomparison (PCMDI) of Lawrence Livermore National Laboratory (http://www-pcmdi.llnl. gov/ipcc/about_ipcc.php). By the time when this study was carried out, outputs from 23 models were submitted, yet not every variable is available for each LME from all the models. This is especially true for ocean variables. In general, there are more archives of the atmospheric variables than of oceanic variables, and more surface variables than three-dimensional variables. Table 1 lists the official model names, country where the modeling group resides, the atmospheric and oceanic model spatial resolution, and the number of realizations available for wind stress (atmospheric variable), sea surface temperature, ocean temperature (oceanic variable) and sea ice concentration for the twentieth-century climate simulations (20C3M).

The models used for AR4 have both improved spatial resolution and physics relative to the previous generation models used for the TAR. The current versions of the atmospheric models features the highest spatial resolution close to 1° in both longitude and latitude, and ocean models with much higher spatial resolution, though generally still not eddy-resolving. Model improvements also include less or no reliance on prescribed restoring forcing (flux adjustment) in the ocean, mobile sea ice, clouds/radiation parameterization, and land/atmosphere fluxes. As for the projections, we choose model runs under the A1B emissions scenario. This scenario is in the middle of the range of those scenarios considered for the AR4 and represents a balance across all sources such as energy source, economic growth, global population and introduction of new and more efficient technologies (Houghton et al., 2001).

## 3. Results

### 3.1. Large scale climate variability patterns of the North Pacific: the PDO

The PDO is the major mode of 20th century North Pacific climate variability on time scales of a decade or longer. (Mantua et al., 1997), as revealed by application of Empirical Orthogonal Function (EOF) analysis of winter SST. The PDO has a general east /west dipole structure in the North Pacific (lower right panel of Fig. 1). By applying EOF analysis to the model simulated SST field for 1901–1999, and the observed SST (the Hadley Center Surface Temperature data set (HadCRUT3v) (http://www.cru.uea.ac.uk/cru/data/temperature/) (Rayner et al., 2003), Overland and Wang (2007a) found that 10 out of 18 models are able to capture the decadal variability in their first EOF structure both spatially and temporally. Fig. 1 is an update from their work, which displays the spatial pattern of the first EOF of SST from 12 models whose spatial correlation with the observed pattern (lower right) is 0.7 or greater. The remaining 11 models have one or more of the following inadequacies: a spatial pattern quite different from the observed one, a peak in the power spectra of the

**Table 1**
List of coupled atmosphere–ocean models and available number of ensemble runs archived for selected variables in 20C3M simulations.

| | IPCC I.D. | Country | Atmosphere resolution | Ocean resolution | Wind stress | SST | Ocean temperature | Sea ice |
|---|---|---|---|---|---|---|---|---|
| 1 | BCCR-BCM2.0 | Norway | 2.8°×2.8°L31 | (0.5–1.5°)×1.5°L35 | | 1 | 1 | 1 |
| 2 | CCSM3 | USA | 1.4°×1.4°L26 | (0.3–1.0°)×1.0°L40 | 9 | 1 | 1 | 7 |
| 3 | CGCM3.1(T47) | Canada | 3.75°×3.7°L31 | 1.9°×1.9°L29 | 5 | 5 | 5 | 5 |
| 4 | CGCM3.1 (T63) | Canada | 2.8°×2.8°L31 | 1.4°×0.9°L29 | 1 | 1 | 1 | 1 |
| 5 | CNRM-CM3 | France | 2.8°×2.8°L45 | 2°×(0.5°–2°)L31 | 1 | | 1 | 1 |
| 6 | CSIRO-Mk3.0 | Australia | 1.875°×1.865°L18 | 1.875°×0.925° L31 | 3 | 3 | 1 | 3 |
| 7 | ECHAM5/ MPI-OM | Germany | 1.875°×1.865°L31 | 1.5°×1.5°L40 | 4 | | | 3 |
| 8 | FGOALS-g1.0 (IAP) | China | 2.8°×2.8°L26 | 1°×1°L30 | 3 | 3 | 3 | 3 |
| 9 | GFDL-CM2.0 | USA | 2.5°×2.0° L24 | 1°×1°L50 | 3 | 3 | 1 | 3 |
| 10 | GFDL-CM2.1 | USA | 2.5°×2.0° L24 | 1°×1°L50 | 3 | 5 | | 5 |
| 11 | GISS-AOM | USA | 4°×3°L20 | 1.4°×1.4°L43 | 2 | 2 | 2 | 2 |
| 12 | GISS-EH | USA | 5°×4°L20 | 2°×2° *cos(lat) L16 | 5 | 5 | 3 | |
| 13 | GISS-ER | USA | 5°×4°L13 | 5°×4°L33 | 9 | 9 | 5 | 9 |
| 14 | INGV-SGX | Italy | 1.125°×1.12°L19 | 1°×1°L33 | 1 | 1 | | 1 |
| 15 | INM-CM3.0 | Russia | 5°×4°L21 | 2°×2.5°L33 | 1 | 1 | | 1 |
| 16 | IPSL-CM4 | France | 3.75°×2.5° L19 | 2°×1°L31 | 1 | 1 | 1 | 1 |
| 17 | MIROC3.2 (hires) | Japan | 1.125°×1.12° L56 | 0.28°×0.188° L47 | 1 | 1 | 1 | 1 |
| 18 | MIROC3.2 (medres) | Japan | 2.8°×2.8°L20 | (0.5°–1.4°)×1.4° L44 | 3 | 3 | 3 | 3 |
| 19 | ECHO-G (MIUB) | Germany/Korea | 3.75°×3.7°L19 | (0.5°–2.8°)×2.8° L20 | 5 | 3 | 3 | 3 |
| 20 | MRI-CGCM2.3.2 | Japan | 2.8°×2.8° L30 | (0.5°–2. 5°)×2° L23 | 3 | 5 | 5 | 5 |
| 21 | PCM | USA | 2.8°×2.8°L18 | (0.5–0.7°)×0.7° L32 | 4 | 1 | | 2 |
| 22 | UKMO-HadCM3 | UK | 3.75°×2.5° L15 | 1.25°×1.25° L20 | 2 | 1 | 1 | 2 |
| 23 | UKMO-HadGem1 | UK | 1.875°×1.25°L38 | (0.33–1.0°)×1.0° L40 | 2 | 2 | | 2 |
| | Total runs | | | | 71 | 57 | 64 | 62 |

Note: The number after letter "L" indicates the number of vertical levels in the model.
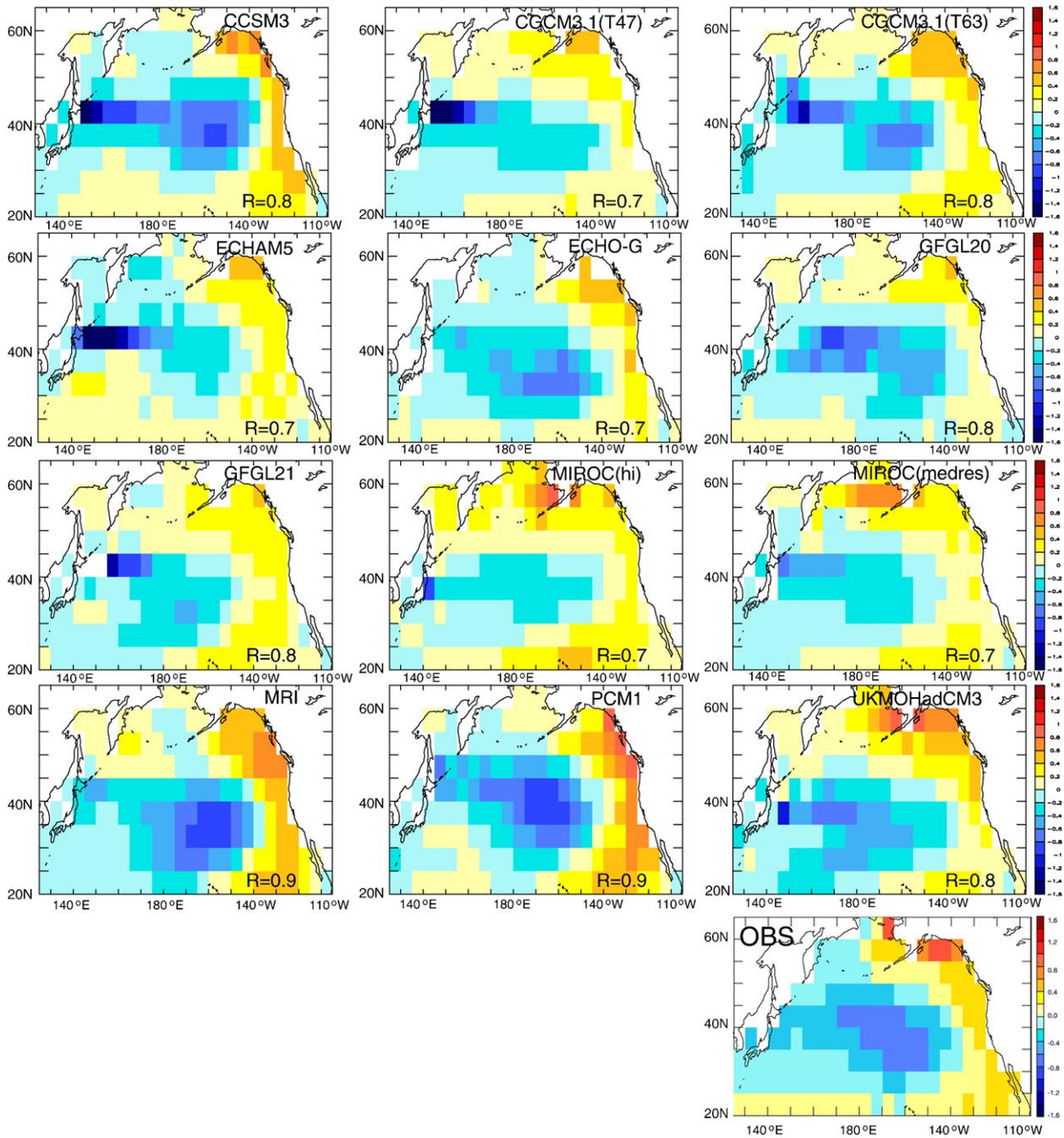
**Fig. 1.** The spatial pattern of the 1st EOF of North Pacific SST for the 20th century based on models. Only those whose spatial correlation with the observed pattern (lower right panel) higher than 0.7 are shown with the correlation coefficients indicated on the lower right corner of each panel. Model names are shown on the top right corner of each panel.
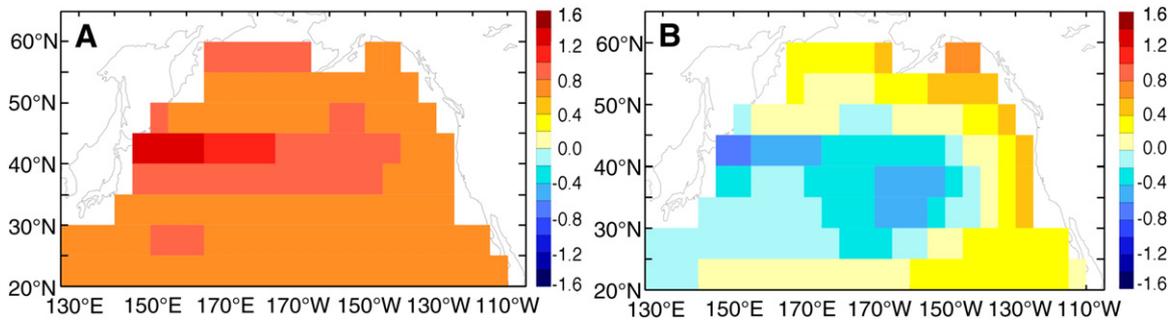


**Fig. 2.** The ensemble means of the projected first (A) and second (B) EOF patterns based on the sub-group of 10 models for the 21st century. The 2nd EOF correlates with the observed PDO pattern at 0.82. (Figure is a modified version of Fig. 1 from Overland and Wang, 2007a).
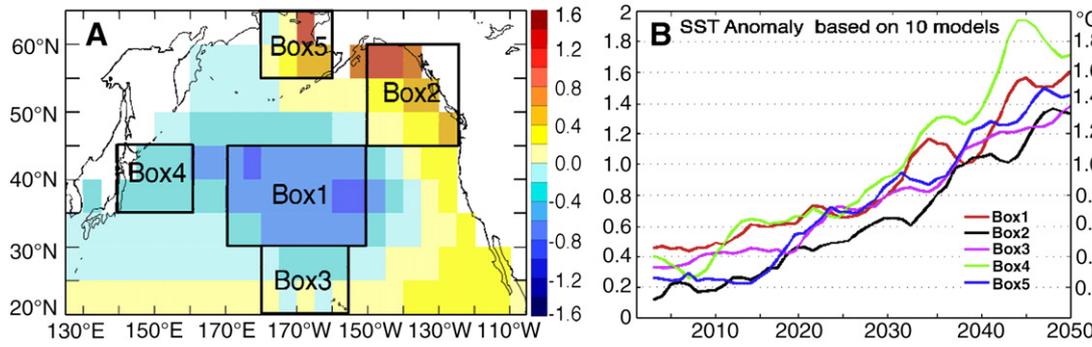
**Fig. 3.** Area-weighted SST anomalies relative to the mea of period 1979–1999 for the selected regions over North Pacific. A) Regions of interest as outlined by the boxes and B) the SST anomalies for each region.

corresponding principal component at a much shorter period than observed, or insufficient variance in the SST fields on interannual and longer time scales. As shown by Overland and Wang (2007a), the first EOF pattern of the SST in the 21st century (2000–2099) is a new, quasi-homogeneous spatial pattern associated with a time series of an upward trend (Fig. 2A). This is true for all the 12 models. The second leading mode (Fig. 2B) of the SST in 21st century is very similar to the observed 20th century PDO pattern. The spatial correlation of the 2nd EOF pattern of 21st century SST with the PDO is 0.82 (Overland and Wang, 2007a). In other words, the influence from the anthropogenic forced trend in SST under the mid range A1B emissions scenario will overpass the natural variability in North Pacific SST in the 21st century, but there will remain the continued presence of the major 20th century pattern of intrinsic climate variability for the North Pacific, i.e. the PDO.

Based on averages over the 10 models, Overland and Wang (2007a) estimated that in less than 50 years the change in winter SST due to anthropogenic influences would surpass the natural variability in most of the North Pacific. Over the central North Pacific, the Gulf of Alaska and along the US west coast this time scale is less certain in that one-half of the models indicate that the interval for the anthropogenic influence to become dominant will be as long as about 90 years, while the other half of the models suggests that this interval will be around 40–50 years. Thus, species in the LMEs that are adapted to the past PDO pattern are liable to experience climate forcing beyond the range of precedent in the historical record as soon as the first half of the 21st century.

The change in the leading mode of North Pacific SST is a reflection of a shift in the nature of the large-scale temperature variability, since the first EOF pattern simply maximizes the variance captured in the analysis. Fig. 3 shows the winter (November to March) temperature
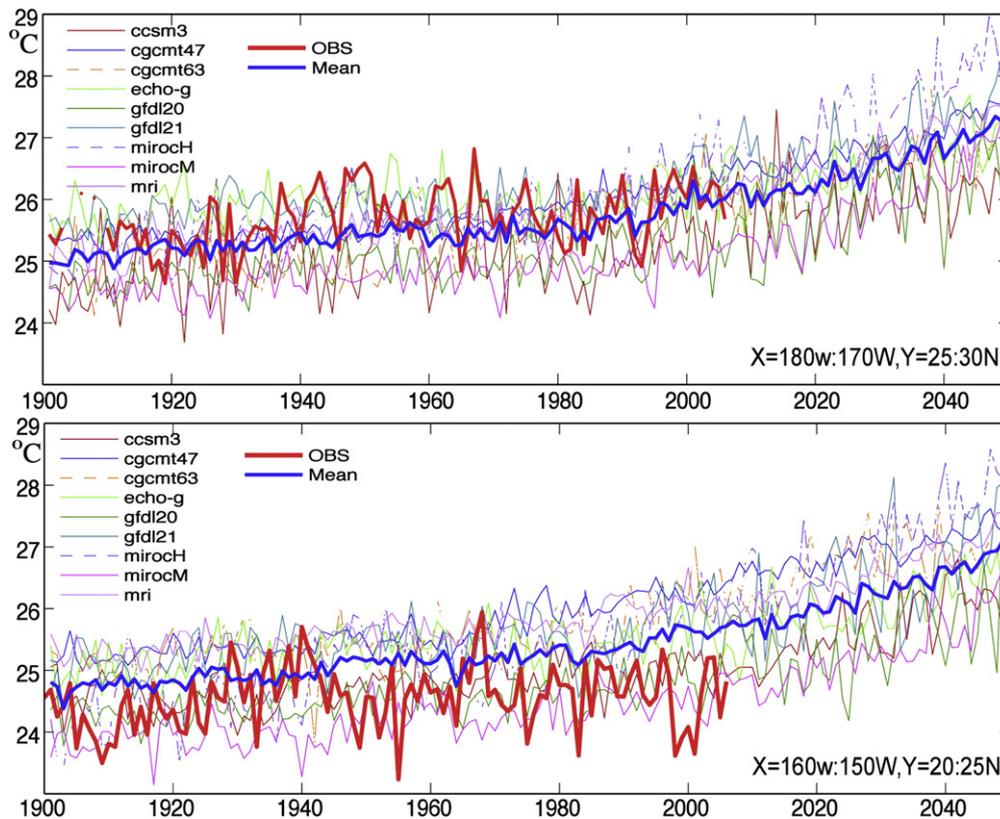


**Fig. 4.** Area-weighted averages of summer (Aug.–Oct.) maximum SAT near Hawaii for 180°–170°W and 25°–30°N, (top) and 160°–150°W and 20°–25°N (bottom) from 1900 to 2050. Thick red line is based on observed dataset (HadCRUt2). The projections are from the group of 9 models with successful representations of the PDO during the 20th century, and are based on emissions scenario A1B. The thick blue line is the model ensemble mean. Solid lines indicate models with more than one realization provided, while dashed lines indicates models with only a single realization.
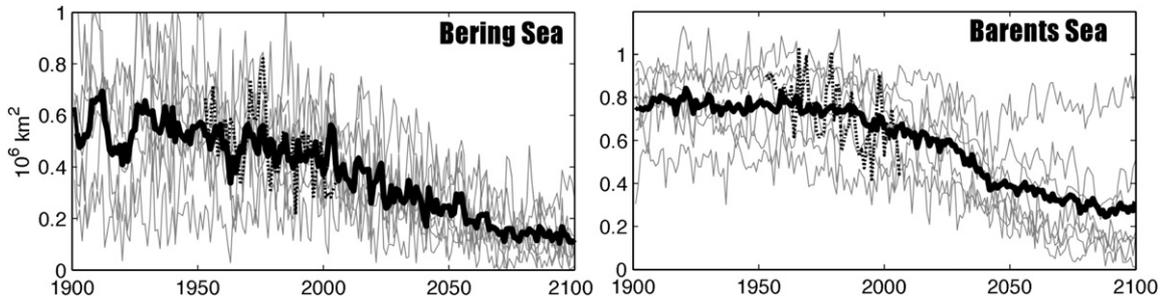
**Fig. 5.** Spring (March and April) sea-ice area integrated over the Bering (left) and the Barents (right) seas for period 1900–2100. Solid thick line indicates the ensemble mean of all the models in the sub-group, and the thick dotted line indicates the observed values based on HadISST1. The thin grey lines are the individual runs from each model.

change relative to 1980–99 period mean projected by the 10 models in 21st century under the A1B emissions scenario. We focus here on five regions: the primary action centers of the PDO (Boxes 1 and 2), an area north of Hawaii (Box 3), the western North Pacific (Box 4) where most models show the largest temperature change in 21st century, and the Bering Sea (Box 5). Quite similar trends of 0.28°, 0.26°, 0.24°, 0.35° and

0.30 °C per decade are found for the five selected regions, respectively. By year 2050 the winter SST anomalies are between 1.3° and 1.7 °C for these regions, with Box 4 (western North Pacific) having the largest increase. The anomalies in Boxes 1 and 4 are systematically greater than the anomalies in Boxes 2 and 5 indicating a trend towards a weaker meridional temperature gradient in the North Pacific region.
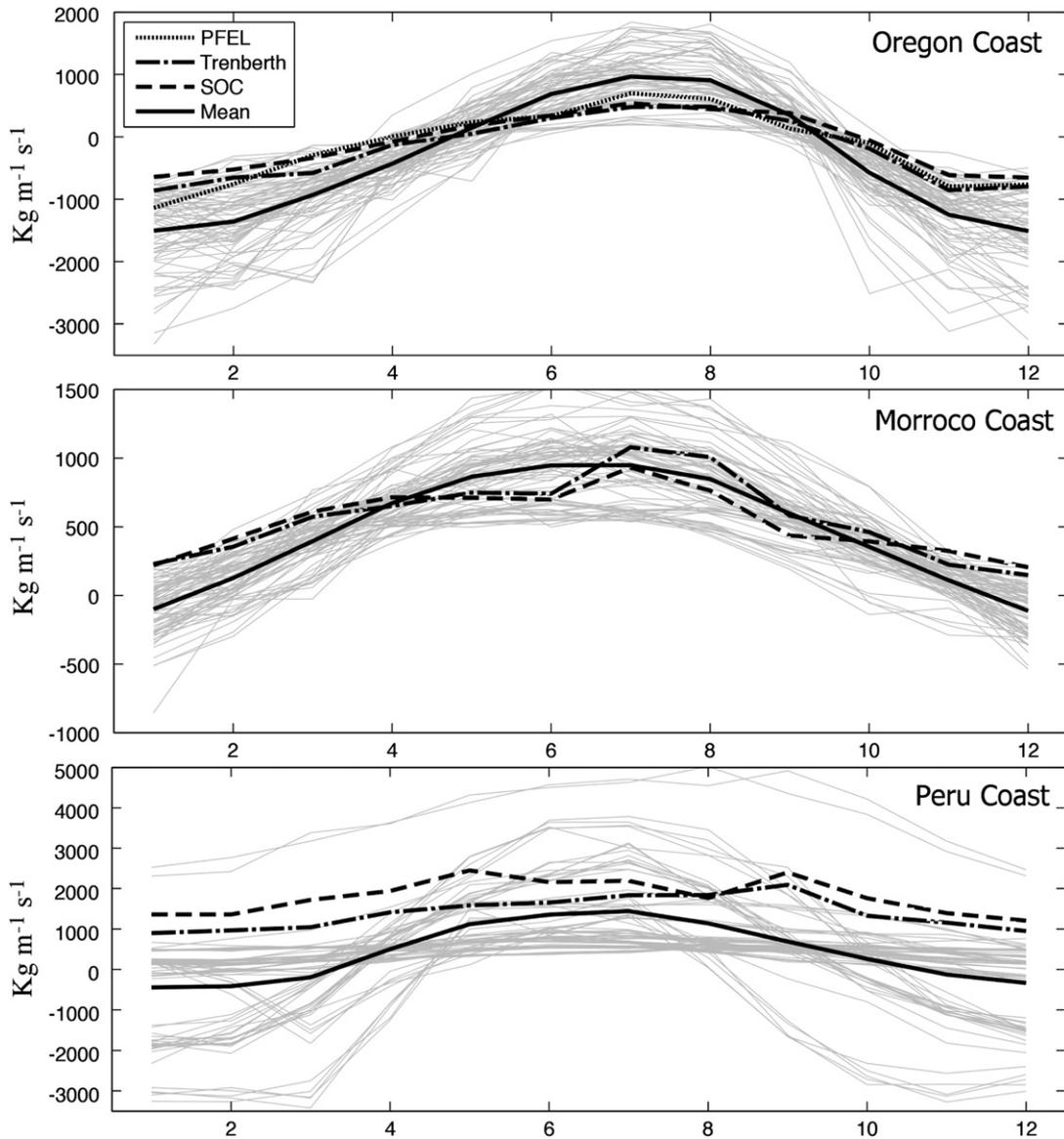


**Fig. 6.** Seasonal cycle of upwelling index along three major eastern boundary currents: top) California Current near Oregon, middle) Canary Current near Morocco, and bottom) Humboldt Current near Peru. The dotted line is the estimated value from the Pacific Fisheries Environmental Laboratory (Pacific Grove, California), and the other two are calculated from the wind stress climatologies from Trenberth (dash-dotted line) and Southampton Oceanography Centre (dashed line), respectively. The thin grey lines are computed based on model simulated wind stress from each ensemble runs averaged over period 1980–1989. The thick solid line is the all-member ensemble mean.

## 3.2. Hawaiian ecosystem

The health of coral reefs near Hawaii is related to the maximum SST they experience in late summer (Hoeke et al., 2006). Projections for this region and for this time of year are complementary to those for the PDO, which are more applicable to basin-scale conditions during winter. The SSTs in late summer (August–October) have been examined for two regions, Area 1 (25°–30°N, 170°–180°W) and Area 2 (20°–25°N, 150°–160°W), northwest of the Hawaiian Islands, which have rich coral reef populations using the 10 models which are able to capture the decadal variability of the North Pacific SST. The area-weighted averages of maximum summer SST for each box from the models are compared with observational data for 1980–1999. Nine out of ten models have their climatology within two standard deviations of the observed value. The other model (UKMO-Hadcm3) yields systematic biases for both boxes, and is therefore excluded from the ensemble mean. Fig. 4 shows the time series of area-weighted averages of maximum SST in the region from the nine remaining model simulations. Model mean changes for both regions are quasi-linear trends of about 0.27 °C per decade in the next century, resulting

in a warming of about 1.3 °C by 2050. One model, Miroc (Hi) (purple dashed line), indicates a substantially greater warming. The ensemble means by these models show slightly different behavior for the two regions. The models are in good agreement with the observations for Area 1, and yield temperatures slightly warmer than the observations for Area 2. This result illustrates that the skill of the models is spatially dependent, which suggests that the reliability of their projections also differs between region (and variables). Part of the reason of the systematic bias in Area 2 can be attributed to the El Niño/Southern Oscillation (ENSO) simulations in these models. The analysis of ENSO in the CMIP3 models has mixed reviews. While there have been some improvements in the last five years, the CMIP3 models still have issues with mean climate, annual cycle and natural variability (e.g. Oldenborgh et al., 2005).

## 3.3. Sea–ice area over the Bering and Barents seas

Seasonal sea–ice cover represents an important feature of the Bering and Barents seas, and is prone to substantial interannual variations (Wang et al., 2007b). The presence of sea ice influences the
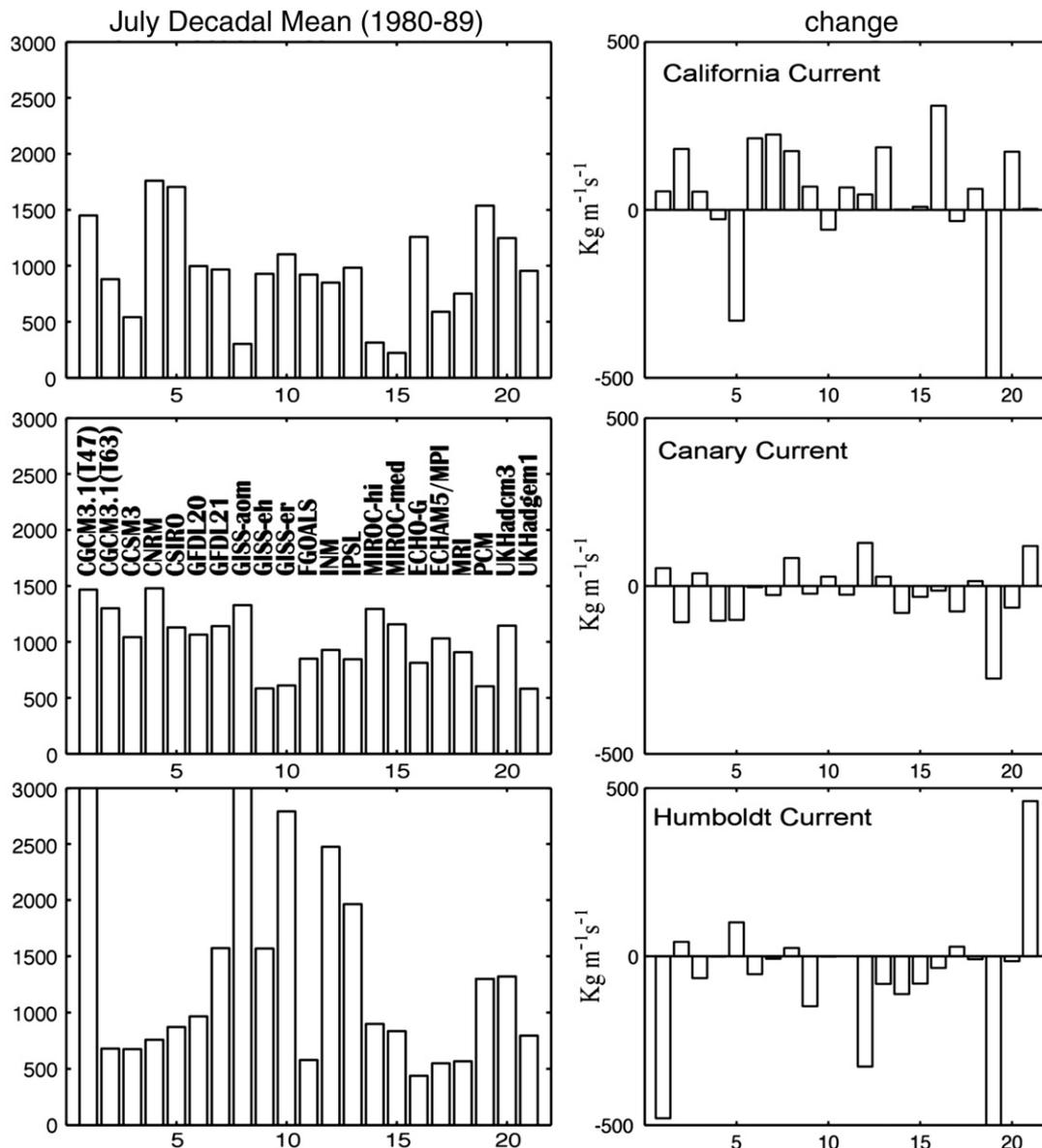


Fig. 7. Decadal mean upwelling indices (left panels) and their modeled possible changes from 1980–1989 to 2030–2039 along three major coastal upwelling systems from top to bottom: California Current near Oregon coast, Canary Current and Humboldt Current.

timing of the spring bloom and bottom temperatures throughout the year. In years with extensive sea ice, the spring bloom tends to occur along the ice edge and this new production ultimately favors benthic communities, which is characteristic of an arctic system. In years of reduced sea–ice coverage, the spring bloom occurs later in association with thermal stratification of the water column; the warmer temperatures at this time allow more efficient grazing by zooplankton thereby favoring pelagic communities characteristic of a sub-arctic system. A shift towards a more sub-arctic system over the last few decades has been documented for the Bering Sea (Grebmeier et al., 2006). The extent of seasonal sea ice in these sub-arctic seas is governed primarily by a balance between advection from the north and melting due to the heat content of the ocean to the south (e.g. Pease, 1980; Overland and Pease, 1982). With regards to the CMIP3 models' ability to simulate sea ice, Overland and Wang (2007b) found good agreement between simulations and observations for the total area of sea ice over the arctic basins in summer (August–September), but fewer models that fit the observations in the seasonal ice zones, such as the Bering Sea and the Barents Sea. It bears noting that the majority of the models had too much ice over the Barents Sea. Retaining their results in averages may lead to bias in estimating sea–ice area in the 21st century. As a result, the projections of the ice area in the Bering and Barents seas are based on a sub-group of seven models that pass the selection criteria (see Table 1 in Overland and Wang, 2007b). All seven models show a continued loss of sea ice in spring (March and April) into the future (Fig. 5), along with considerable interannual variability, a characteristic of northern systems. The single realizations from individual models (grey lines) illustrate the combination of large natural variability on top of the trend due to global warming (solid thick line). One significant feature in the sea–ice projection over the two sub-arctic seas is the increased rate of ice reduction in 21st century compared with 20th century, particularly over the Barents Sea. The projected linear trend of the sea–ice area over the Bering Sea in the first half of 21st century is comparable with the observed trend in the satellite era. The ensemble means (sold thick line) indicate a reduction in the ice area of about 43% and 36% from 1980–1999 to 2045–2055 for the Bering and Barents seas, respectively.
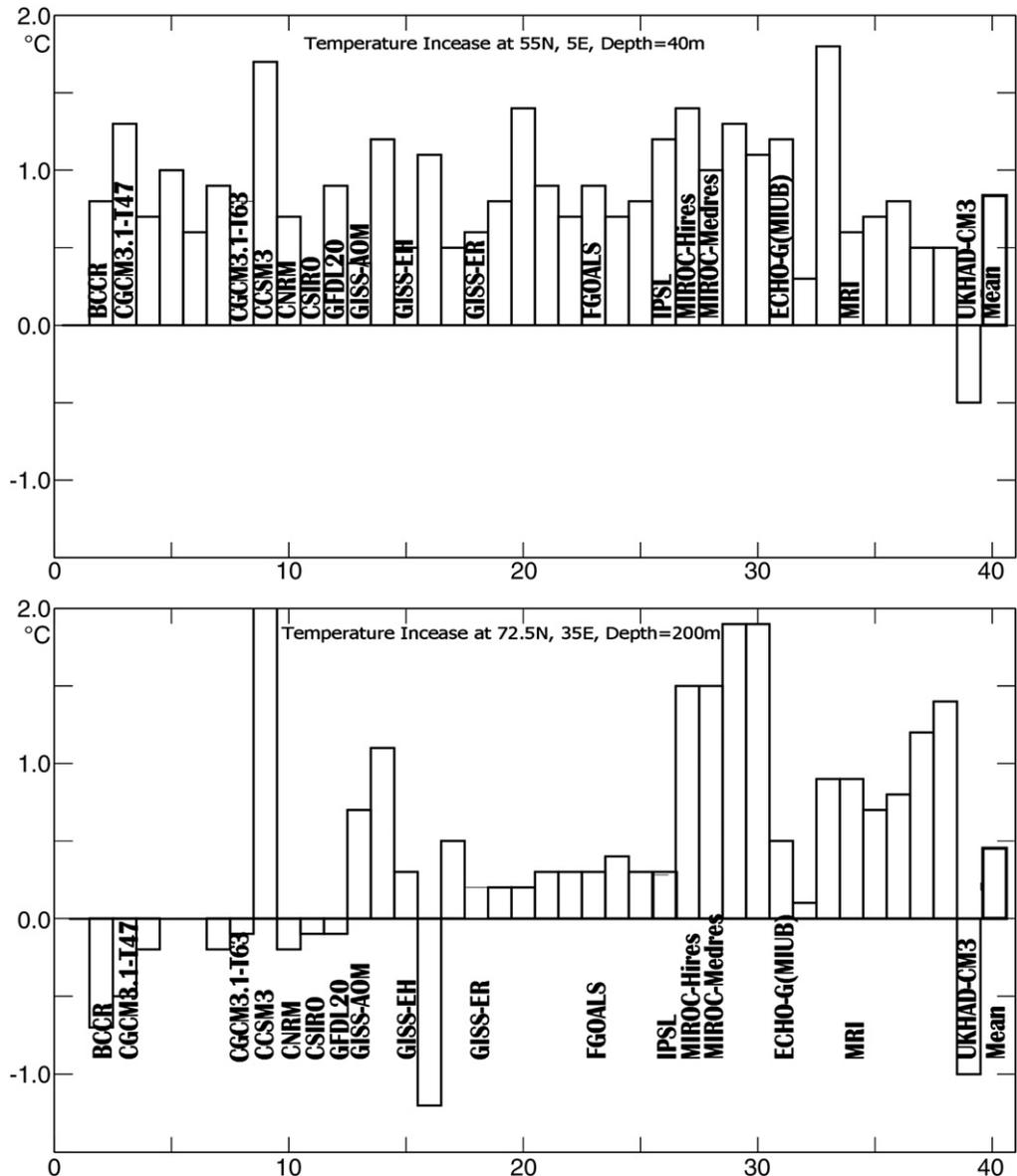


**Fig. 8.** Modeled near-bottom temperature change at selected locations (North Sea: 55°N, 5°E, top, and Barents Sea: 72.5°N and 35°E, bottom) between 2030–2039 and 1990–1999 under the A1B scenario from the available models. Each bar represents one realization from the multiple ensemble runs. The model name is marked on the 1st bar to the left if multiple runs are provided. The last bar in each panel shows the all-model ensemble mean.

## 3.4. Upwelling systems

Coastal upwelling provides a sustained source of nutrients to the upper ocean, thereby supporting some of the most productive fisheries in the world, particularly for small pelagic species. It is of interest therefore to examine the potential future changes in upwelling in various locations. For the purposes of the present study, we consider the along-shore component of the wind stress, which is proportional to the cross-shore Ekman transport and the vertical mass flux through the base of the oceanic Ekman layer. The model simulations of the along-shore wind stress are used to compute upwelling indices for three eastern boundary currents: (1) the California Current off the coast of Oregon, USA (45°N, 125°W), (2) the Canary Current off the coast of Morocco, Africa (30°N, 14°W), and (3) the Humboldt Current off the coast of Peru, South America (11°S, 79°W). As there are no direct observations of wind stress, we used the climatology of the wind stress, calculated from the surface winds from the European Centre for Medium Range Weather Forecast (ECMWF) for 7 years (1980–86) (Trenberth et al., 1989) and the global analysis based on in situ reports for the period 1980–93 from the Southampton Oceanography Centre (SOC), United Kingdom (Josey et al., 1999). For the California Current location, we also used the monthly upwelling index provided by the Pacific Fisheries Environmental Laboratory (PFEL) (http://www.pfeg.noaa.gov/products/PFEL/modeled/indices/upwelling/upwelling.html).

As a first step in evaluating the model results, we constructed monthly climatologies of the upwelling index at the three locations (Fig. 6). This exercise revealed that most of the models could approximately reproduce the correct seasonal cycle in the upwelling index along the California and Canary currents (Fig. 6 top and middle) with the strongest positive upwelling in the summer (June to August). Yet they tend to overestimate the magnitude of this seasonal cycle. Moreover, there was large variation in the model simulated climatology between the individual models, especially for the Humboldt Current location (Fig. 6 bottom). Fig. 6 displays the complexity in evaluating the models' performance. The models' inability to correctly simulate upwelling, at least directly, is not that surprising. The upwelling winds in these coastal regions are strongly influenced by the local pressure gradient, which in turn reflects land–sea temperature contrasts, particularly during summer. Due to their coarse spatial resolutions, the models should not be expected to reproduce the nuances of the coastal weather even though, as shown earlier, many of them are able to capture larger-scale and open-ocean features of the atmosphere–ocean system and its variability. At this point we did not screen the models for their sub-grid scale phenomenon, which the climate models were not designed to be able to simulate and the upwelling projections are based on ALL available model outputs.

Fig. 7 displays the decadal averaged upwelling index for July at each coastal region (left panels) and their projected changes from 1980–89 to 2030–39 (right panels). For the California Current region, seventeen models predict increases in July upwelling with only two models (CSIRO-mk3.0 and PCM) indicating substantial decreases. On the other hand, mixed projections are found in upwelling for the Canary and Humboldt Currents, with the largest model spread for Humboldt Current. Given the inherent limitations of the models to properly handle upwelling, the projections from the present analysis are highly uncertain, and further analysis is warranted. Potentially the CMIP3 model simulations can be used to estimate changes in upwelling through an indirect method, as will be elaborated upon in the concluding section.

## 3.5. Bottom ocean temperature in Barents and North seas

The final variable considered is the bottom temperature in the northern portion of the North Sea and the eastern portion of the Barents Sea. These regions represent the southern and northern limits of cod in the eastern North Atlantic. While cod respond to a range of oceanic factors, they are sensitive to water temperature and can be found in regions with annual temperatures from 0°–12 °C (Drinkwater, 2005). A complication arises in analysis of the simulated bottom temperatures in these two shelf regions due to differences in the models' bathymetry. Therefore, we used a common depth of 40 m for the North Sea and 200 m for the Barents Sea to represent near-bottom temperatures. Due to the lack of available observations to us at the time of writing, we were not able to validate the models' simulations. We therefore examine the projections by ALL the available models that have sub-surface ocean temperature archives.

Fig. 8 shows the difference in mean temperature between the decades of 2030–39 and 1990–99 from each model. The results for the North Sea (top panel) show model averaged mean warming of 0.8 °C, with consistency between individual models and their ensemble members. This magnitude of warming is in the range of possible ecological impacts. The results for the Barents Sea (lower panel) also indicate warming, but with considerably spread among the models. In particular, these results suggest two different possible scenarios: minor (but largely positive) changes by 10 models, and increases of more than 1 °C from eight realizations of five models. Since the location selected here (72.5°N, 35°E) is beyond the current range of cod, the possibility of a major warming suggests the potential for cod colonization.

## 4. Discussion and summary

We have analyzed CMIP3 model simulations with a focus on elements of the atmosphere–ocean system relevant to several LMEs. Our method has been to critically evaluate individual model simulations for the 20th century in terms of their fidelity at replicating the observed climatology and/or variability, and then to use a subset of the better models for projecting changes into the 21st century. The model validation component of the analysis indicates that the confidence level is higher in projections of large-scale patterns of North Pacific SST and sea–ice extent, but lower in projections of local forcing, such as coastal upwelling in eastern boundary current regions. This result indicates that a more complete analysis is necessary in these local regions than provided by the overall survey conducted in the IPCC AR4.

A series of analyses was carried out on North Pacific SST. Projections based on a sub-group of the models that reproduced the observed spatial and temporal character of the PDO during the 20th century indicate that a spatially homogeneous and linear warming trend of the North Pacific SST will be the leading mode of variability in the 21st century, with decadal variability resembling the PDO as the 2nd mode of variability. The warming due to the trend will be as large as the magnitude of the PDO around 2050 in most of the North Pacific. In other words, the North Pacific, at least in terms of its SST, is liable to be in an unprecedented state in a few decades, with presumably major implications for the ecosystem. The models projections for selected regions in the North Pacific indicate consistency in the warming trends with some hint towards a weaker meridional SST gradient across the North Pacific in winter. The sub-group of models also projected about 1.2 °C of warming in summertime SST northwest of Hawaii, with large inter-annual variability on top of that, which appears to be crucial to coral reef health. While the model results suggest a relatively high degree of confidence in projections for North Pacific SST fields, there are some caveats. It is known that the North Pacific atmosphere–ocean system is sensitive to the changes in ENSO in the tropical Pacific (e.g., Newman et al., 2003), which the global climate models, in general, do not fully represent. There have been recent improvements, but the models still have errors in their handling of the seasonal mean climate of the tropics and the structure of ENSO (e.g., Oldenborgh et al., 2005; Delworth et al., 2006; Collins et al., 2006), and these limitations need to be recognized in interpretation of their simulations for the North Pacific.

Roughly one-third of the models were able to reproduce the maximum ice extent in the Bering and Barents seas close to observations

for the last twenty years of the 20th century. These models indicate continued declines in spring sea ice extent into the 21st century, amounting to roughly 40% reduction by 2050.

As mentioned above, the results for coastal upwelling are equivocal. The models apparently overestimated the magnitude of mean seasonal cycle of the upwelling along the California and Canary currents. Nevertheless, there may be an indirect way to anticipate potential changes in this locally important mechanism. In particular, in an analysis of seasonally-delayed upwelling in 2005 along the Oregon coast (one of the locations considered in the present study), Schwing et al. (2006) show that interannual variations in upwelling correspond with broadscale anomalies in sea-level pressure, in particular the strength of the subtropical High to the west of the coast. Changes in this kind of structure, in principle, can be handled properly by coarse-resolution climate models, which could then be used as an index for coastal upwelling. This suggestion is tentative; its justification requires further analysis.

Bottom temperatures in shelf regions such as the North and Barents Sea also reflect regional processes (e.g., currents) and hence their simulation might be expected to include relatively high uncertainty. The models show some consistency for the North Sea, with a mean warming of ~0.8 °C over a 40-year period into the 21st century, but considerably more scatter in projected changes for the Barents Sea. This seems to be consistent with the finding by Chapman and Walsh (2007), who showed that models have the largest bias in their simulated surface air temperature and sea level pressure over the Barents Sea region in the 20th century.

Our findings support the CMIP3 models as a useful source for climate projections on regional scales for marine ecosystem interests. Care must be exercised in their application with respect to selecting a reliable subset of models when extracting relevant variables in that not all models are equally reliable. Therefore, it is probably good practice to exclude models that clearly do not characterize a system properly to the extent this can be determined given limited data sets for validation. It is also a good idea to retain as many models as possible to form an ensemble forecast in order to reduce the errors intrinsic to individual models and provide important information on the uncertainty in these projections on the whole.

## Acknowledgments

## References

Beamish, R.J., 1993. Climate and exceptional fish production off the west coast of North America. Canadian Journal of Fisheries and Aquatic Sciences 50, 2270–2291.

Chapman, W.L., Walsh, J.E., 2007. Simulations of Arctic temperature and pressure by global coupled models. Journal of Climate 20, 609–632.

Clark, W.G., Hare, S.R., 2002. Effects of climate and stock size on recruitment and growth of Pacific Halibut. North American Journal of Fisheries Management 22, 852–862.

Collins, W.D., Bitz, C.M., Blackmon, M.L., Bonan, G.B., Bretherton, C.S., Carton, J.A., Chang, P., Doney, S.C., Hack, J.J., Henderson, T.B., Kiehl, J.T., Large, W.G., McKenna, D.S., Santer, B.D., Smith, R.D., 2006. The Community Climate System Model Version 3 (CCSM3). Journal of Climate 19, 2122–2143.

Delworth, T.L., Rosati, A., Stouffer, R.J., Dixon, K.W., Dunne, J., Findell, K., Ginoux, P., Gnanadesikan, A., Gordon, C.T., Griffies, S.M., Gudgel, R., Harrison, M.J., Held, I.M., Hemler, R.S., Horowitz, L.W., Klein, S.A., Knutson, T.R., Lin, S.-J., Milly, P.C.D., Ramaswamy, V., Schwarzkopf, M.D., Sirutis, J.J., Stern, W.F., Spelman, M.J., Winton, M., Wittenberg, A.T., Wyman, B., 2006. GFDL's CM2 Global Coupled Climate Models. Part I: formulation and simulation characteristics. Journal of Climate 19, 643–674.

Drinkwater, K.F., 2005. The response of Atlantic cod to future climate change. ICES Journal of Marine Science 62, 1327–1337.

Grebmeier, J.M., Overland, J.E., Moore, S.E., Farley, E.V., Carmack, E.C., Cooper, L.W., Frey, K.E., Helle, J.H., McLaughlin, F.A., McNutt, S.L., 2006. A major ecosystem shift in the Northern Bering Sea. Science 311, 1461–1464.

Hare, S.R., Mantua, N.J., Francis, R.C., 1999. Inverse production regimes: Alaska and west coast Pacific Salmon. Fisheries 24, 6–14.

Hoeke, R., Brainard, R., Moffitt, R., Merrifield, M., 2006. The role of oceanographic conditions and reef morphology in the 2002 coral reef bleaching event in the Northwestern Hawaiian Islands. Atoll Research Bulletin 543, 489–504.

Houghton, J.T., Ding, Y., Gridds, D.J., Noguer, M., van der Linden, P.J., Dai, X., Maskell, K., Johnson, C.A. (Eds.), 2001. Climate Change 2001: The Scientific Basis. Cambridge University Press. 881 pp.

Josey, S., Kent, E., Taylor, P., 1999. New insights into the ocean heat budget closure problem from analysis of the SOC air–sea flux climatology. Journal of Climate 12, 2856–2880.

Livingston, P.A., Tjelmeland, S., 2000. Fisheries in boreal ecosystems. ICES Journal of Marine Science 57, 619–627.

Mantua, N.J., Hare, S.R., Zhang, Y., Wallace, J.M., Francis, R.C., 1997. A Pacific interdecadal climate oscillation with impacts on salmon production. Bulletin of the American Meteorological Society 78, 1069–1079.

Newman, M., Compo, G.P., Alexander, M.A., 2003. ENSO-forced variability of the Pacific Decadal Oscillation. Journal of Climate 16, 3853–3857.

Oldenborgh, G.J., Philip, S., Collins, M., 2005. El Niño in a changing climate: a multi-model study. Ocean Science Discussions 2, 267–298.

Overland, J.E., Pease, C.H., 1982. Cyclone climatology of the Bering Sea and its relation to sea ice extent. Monthly Weather Review 110, 5–13.

Overland, J.E., Wang, M., 2007a. Future climate of the North Pacific Ocean. EOS Transactions of the AGU 88 (178), 182.

Overland, J.E., Wang, M., 2007b. Future regional Arctic Sea ice declines. Geophysical Research Letters 34 (17), L17705. doi:10.1029/2007GL030808.

Pease, C.H., 1980. Eastern Bering Sea ice processes. Monthly Weather Review 108, 2015–2023.

Pierce, D.W., 2004. Future changes in biological activity in the north Pacific due to anthropogenic forcing of the physical environment. Climatic Change 62, 389–418.

Rayner, N.A., Parker, E., Horton, E.B., Folland, C.K., Alexander, L.V., Rowell, D.P., Kent, E.C., Kaplan, A., 2003. Global analyses of sea surface temperature, sea ice, and night marine air temperature since the late nineteenth century. Journal of Geophysical Research 108, 4407. doi:10.1029/2002JD002670.

Schwing, F.B., Bond, N.A., Bograd, S.J., Mitchell, T., Alexander, M.A., Mantua, N., 2006. Delayed coastal upwelling along the U.S. West Coast in 2005: a historical perspective. Geophysical Research Letters 33, L22S01. doi:10.1029/2006GL026911.

Sundby, S., 2000. Recruitment of Atlantic cod stocks in relation to temperature and advection of copepod populations. Sarsia 85, 277–298.

Trenberth, K., Olson, J., Large, W., 1989. A Global Ocean Wind Stress Climatology Based on ECMWF Analyses. National Center for Atmospheric Research, Boulder, Colorado. Technical Report NCAR/TN-338+STR.

Wang, M., Overland, J.E., Kattsov, V., Walsh, J.E., Zhang, X., Pavlova, T., 2007a. Intrinsic versus forced variation in coupled climate model simulations over the Arctic during the 20th century. Journal of Climate 20, 1093–1107.

Wang, M., Bond, N.A., Overland, J.E., 2007b. Comparison of atmospheric forcing in four sub-arctic seas. Deep-Sea Research II 54, 2543–2559.